Redox Biology 30 (2020) 101432

Contents lists available at ScienceDirect

Redox Biology

journal homepage: www.elsevier.com/locate/redox

Enhanced cardiomyocyte reactive oxygen species signaling promotes ibrutinib-induced atrial fibrillation

Xinyu Yang[a,b], Na An[a,b], Changming Zhong[a], Manke Guan[a], Yuchen Jiang[b], Xinye Li[b], Hanlai Zhang[a], Liqin Wang[a], Yanfei Ruan[c], Yonghong Gao[a], Nian Liu[c,**], Hongcai Shang[a,***], Yanwei Xing[b,*]

[a] Key Laboratory of Chinese Internal Medicine of the Ministry of Education, Dongzhimen Hospital Affiliated to Beijing University of Chinese Medicine, Beijing, 100700, China
[b] Guang'anmen Hospital, China Academy of Chinese Medical Sciences, Beijing, 100053, China
[c] Department of Cardiology, Beijing An Zhen Hospital of the Capital University of Medical Sciences, Beijing, 100853, PR China

ARTICLE INFO

Keywords:
Reactive oxygen species
Ibrutinib
Atrial fibrillation
Electrical remodeling
Structural remodeling

ABSTRACT

Atrial fibrillation (AF) occurs in up to 11% of cancer patients treated with ibrutinib. The pathophysiology of ibrutinib promoted AF is complicated, as there are multiple interactions involved; the detailed molecular mechanisms underlying this are still unclear. Here, we aimed to determine the electrophysiological and molecular mechanisms of burst-pacing-induced AF in ibrutinib-treated mice. The results indicated differentially expressed proteins in ibrutinib-treated mice, identified through proteomic analysis, were found to play a role in oxidative stress-related pathways. Finally, treatment with an inhibitor of NADPH oxidase (NOX) prevented and reversed AF development in ibrutinib-treated mice. It was showed that the related protein expression of reactive oxygen species (ROS) in the ibrutinib group was significantly increased, including NOX2, NOX4, p22-phox, XO and TGF-β protein expression. It was interesting that ibrutinib group also significantly increased the expression of ox-CaMKII, *p*-CaMKII (Thr-286) and *p*-RyR2 (Ser2814), causing enhanced abnormal sarcoplasmic reticulum (SR) Ca^{2+} release and mitochondrial structures, as well as atrial fibrosis and atrial hypertrophy in ibrutinib-treated mice, and apocynin reduced the expression of these proteins. Ibrutinib-treated mice were also more likely to develop AF, and AF occurred over longer periods. In conclusion, our study has established a pathophysiological role for ROS signaling in atrial cardiomyocytes, and it may be that ox-CaMKII and *p*-CaMKII (Thr-286) are activated by ROS to increase AF susceptibility following ibrutinib treatment. We have also identified the inhibition of NOX as a potential novel AF therapy approach.

1. Introduction

Ibrutinib is a Bruton's tyrosine kinase (Btk) inhibitor that is authorized by the US Food and Drug Administration (FDA) for clinical use in the treatment of chronic lymphocytic leukemia (CLL), mantle cell lymphoma, and Waldenstrom macroglobulinemia as a monotherapy or as part of a combination therapy [1–3]. In a previous clinical trial, ibrutinib substantially improved the survival rates of patients compared to those treated with ofatumumab [3,4]. Although ibrutinib shows slightly less toxicity relative to other routine chemotherapy-based treatments, it is a chronic medication that is usually used for long-term treatment [5]. Evidence indicates that ibrutinib can increase the risk of bleeding, as well as the incidence of atrial fibrillation (AF) [6]. The reported incidence of nascent AF in patients treated with ibrutinib is as high as 11% [7], and ibrutinib has been shown to be related to an approximately four-fold increase in the risk of developing AF [8–10]. Therefore, patients treated with ibrutinib pose a greater challenge in clinical practice. In a randomized trial (RESONATE) comparing the effects of ibrutinib with those of ofatumumab in patients with CLL, incident Common Terminology Criteria for Adverse Events (CTCAE) grade 3 AF was identified in 3% of patients treated with ibrutinib compared to 0% of patients treated with ofatumumab [6].

Among the 33 million patients with AF globally, many suffer from not only harmful symptoms and a decline in quality of life, but also

* Corresponding author.
** Corresponding author.
*** Corresponding author.
E-mail addresses: liunian1973@hotmail.com (N. Liu), shanghongcai@126.com (H. Shang), xingyanwei12345@hotmail.com (Y. Xing).

https://doi.org/10.1016/j.redox.2020.101432
Received 13 November 2019; Received in revised form 27 December 2019; Accepted 12 January 2020
Available online 20 January 2020

have a five-fold increased risk of stroke and a twofold increased risk of death [11–13]. AF reduces cardiac output, which may lead to cardiac failure, and facilitates atrial thrombus formation, which can result in stroke and arterial embolization [10]. The pathophysiology of ibrutinib-induced AF promotion is complicated, and involves multiple cellular and molecular interactions; the detailed molecular mechanisms underlying AF development have not yet been determined. The phosphoinositide 3-kinase (PI3K)-Akt pathway is an important cardioprotective pathway that plays a role in the B cell receptor (BCR) signaling cascade [14]. McMullen et al. [15] assessed PI3K expression in an experimental model of rat myocytes and determined that exposure to ibrutinib resulted in reduced P13K expression, indicating an increased risk of developing AF. More recently, Jiang et al. [16] reported that the inhibition of CaMKII may be a therapeutic strategy for the prevention and cure of ibrutinib-treated mice. Other studies have found that the multifunctional CaMKII as an ROS sensor [17] and a proarrhythmic signal [18]. Ox-CaMKII could be a biomarker and pro-arrhythmic signal for connecting increased atrial ROS to AF [17,19,20]. However, it is still not clear whether the CaMKII-RyR2 pathway is activated by increased ROS induced by ibrutinib to develop AF susceptibility. Therefore, we established a mouse model of AF susceptibility using esophageal burst stimulation, and performed proteomics analysis to explore for the first time the role of ROS in ibrutinib-treated mice. A further aim of the present study was to identify a potential novel therapeutic approach to treat AF.

2. Materials and methods

2.1. Animal model and administration of drugs

Ninety-five male C57BL/6 21–28-day-old mice (body weight ~20 g) were purchased from the Vital River Experimental Animal Center (VREAC, Beijing, China). Using a table of random numbers, fifty of the animals were divided into two groups: the control group (n = 25) and the ibrutinib group (n = 25). The ibrutinib group received an intraperitoneal injection of 30 mg/kg ibrutinib once a day [21]. Mice were dosed with ibrutinib or vehicle at the same time each day. After 14 days of administration, the animals were subjected to esophageal burst stimulation, followed by ECG recording, echocardiography test, pathological staining, electron microscopy, calcium imaging, mitochondrial ROS production measurement, and proteomics analysis. Then, we used apocynin (20 μl 20 μM, Sigma Aldrich, St. Louis, MO, USA), an inhibitor of NOX [22] for drug administration, and mice were divided into three groups: the control group (n = 15), the ibrutinib group (n = 15) and the apocynin group (n = 15). Two weeks after administration, the animals were subjected to esophageal burst stimulation, electrocardiograms were recorded, and then calcium release was detected and western blotting was performed. All animals used in our study received humane care in accordance with the Health Guide for the Care and Use of Laboratory Animals. This study was approved by the Animal Care Committee of Dongzhimen Hospital Affiliated to Beijing University of Chinese Medicine.

2.2. Establishment of the AF model

Mice electrophysiological studies were performed as previously described [23–25]. Briefly, all mice were anaesthetized with an intraperitoneal injection of 1% pentobarbital sodium, and surface limb lead ECGs were recorded on each limb. The electrode was inserted through the esophagus near the left atrium (LA), and ECGs were recorded using PowerLab and LabChart 7 software. Both programmed electrical stimulation (PES) and burst pacing (2 ms at 50 Hz) were used to determine their susceptibility to pacing-induced AF [23,24]. AF in ibrutinib-treated mice was identified through differentiation from the normal sinus rhythm if the ECGs showed a lack of regular P waves. Restored sinus rhythm in burst-pacing-induced AF mice was identified through the detection of P waves. The duration of AF was recorded in each animal.

2.3. Echocardiography

As described previously [26], Vevo 2100 Imaging System (FUJIFILM VisualSonics, Inc., USA; probe, MS-550D; frequency, 40 MHz) was used to detect cardiac structural and functional indicators. First, each group of mice was anaesthetized with ether. After successful anesthesia, the mice in each group were fixed on their backs; their fur was shaved and their skin was cleaned, and then heart structural and functional indicators were examined. Ultrasound measurements were performed to determine the LA diameter, LA area, left ventricular internal dimension systole (LVIDs) and E/A peak. Echocardiography was performed by a technician who was blind to the grouping of the mice.

2.4. Myocardial histopathology

The left atrial tissue was fixed in 4% paraformaldehyde, and serially sectioned. The sections were dyed with Masson's trichrome stain, and Sirius red dye, and evaluated by light microscopy and polarized light microscopy [27]. The hearts of three mice were stained and analyzed in each group. The macroscopic changes in the mice hearts were evaluated by optical microscopy. The samples were observed at 40 × , and longitudinal cutting samples were tested in each sample. Finally, Image-Pro 6.0 software was used for quantitative analysis of images.

2.5. Electron microscopy

The left atrial tissue in each group was immobilized by retrograde aortic perfusion with 2.5% glutaraldehyde [28,29]. Three hearts were immobilized and analyzed in the control group and the ibrutinib group, respectively. Furthermore, the myocardial tissues of mice were routinely processed and observed using transmission electron microscopy (H-600, Japan) as previously described [30].

2.6. Cell preparation and solutions

Atrial myocytes were separated using an established enzyme digestion protocol [31]. Isolated atrial myocytes were placed in a dish containing laminin-coated to promote atrial myocytes adherence. Solution containing 140 mM NaCl, 4 mM KCl, 2 mM $CaCl_2$, 1 mM $MgCl_2$, 10 mM HEPES and 5 mM glucose (pH 7.3–7.4) was added to the dishes at room temperature, and then Ca^{2+} measurement was performed.

DL-Dithiothreitol (DTT; Sigma Aldrich), an inhibitor of ibrutinib, was dissolved in 100 mM normal saline and stored at 4 ˚C. Apocynin was dissolved in 100 μM dimethyl sulfoxide (DMSO) and stored at 4 ˚C.

2.6.1. Cardiomyocyte Ca^{2+} imaging

Isolated atrial myocytes were incubated with 5 μmol/L Fluo-4 AM (Invitrogen, Carlsbad, CA, USA). The IonOptix system (IonOptix, Westwood, MA, USA) was used to record transient changes in Ca concentrations, and Ca^{2+} sparks were recorded by laser scanning confocal microscopy (Leica Microsystems, Wetzlar, Germany). In the control and ibrutinib groups, field stimulation at 1 Hz was performed for at least 20s to attain a steady state, and the calcium waves and frequency of Ca^{2+} sparks were acquired over a 10-s rest period. Furthermore, isolated atrial myocytes were incubated in NT solution (control group), NT supplemented with 0.5 mM ibrutinib (ibrutinib group) [32], and NT supplemented with 0.5 mM ibrutinib with 100 μM apocynin (apocynin group) [33] for 30 min. At 1 Hz–3 Hz, the changes of calcium transient and Ca^{2+} sparks were recorded in the ibrutinib group and apocynin group.

2.6.2. Measurement of mitochondrial ROS generation

MitoSOX Red (Invitrogen) was used to detect mitochondrial ROS

generation [34]. Isolated atrial myocytes were incubated with MitoSOX Red (5 μM) in NT solution (Control group), NT with 0.5 mM ibrutinib (ibrutinib group), and NT with 0.5 mM ibrutinib with 10 mM DTT (ibrutinib + DTT group) for 120 min at room temperature [35]. The intensity of red fluorescence was measured in five different regions of each cell. The baseline MitoSOX red fluorescence intensity (100%) was acquired based on mean control cell values.

2.7. Proteomics

The left atrial tissue removed from the liquid nitrogen was transferred to low protein binding tubes and lysed with 1 mM phenylmethylsulfonyl fluoride (PMSF). Next, samples were further lysed by sonication. After sonication, the samples were centrifuged at 12,000 × *g* for 10 min, and the supernatant was collected. This was then repeated once. The protein concentration was determined using the bicinchoninic acid (BCA) protein assay [36], and samples were stored at −80 °C. Each sample protein was then isolated using 12% SDS-PAGE. Then, the gel was stained with Coomassie Brilliant Blue according to the protocol of Candiano [37]. First, the gel sample protein was fixed for 2 h and stained for 12 h. After staining, the gel was washed with water until the bands were visualized. Finally, the stained gel was scanned with Image Scanner (GE Healthcare, Chicago, IL, USA) at a resolution of 300 dpi. The Filter Aided Sample Preparation (FASP) method was used to analyze the bands [38]. Some proteins were trypsinized and labeled, and then the same amount of each labeled sample was mixed and subjected to chromatography. Finally, the sample was subjected to liquid chromatography-tandem mass spectrometry (LC-MS/MS). Proteome Discoverer (v2.2) (Thermo Fisher Scientific, Waltham, MA, USA) was used to comprehensively identify all Q Exactive MS/MS raw data against the sample protein database.

2.8. Western blotting

The left atrial tissue from liquid nitrogen was collected and lysed in the RIPA buffer. Protein content was quantified with the BCA reagent kit. Protein samples from each group were separated by 10% SDS-PAGE and then transferred to PVDF membranes (Millipore, Billerica, MA, USA). After incubation in closed buffer (0.5% Tween-20 in TBS, 5% bovine serum albumin (BSA)), the membrane was incubated with the following antibodies for 1 h at room temperature: anti-calmodulin-dependent protein kinases II (CaMKII, ab181052), anti-CaMKII (phospho T286, ab32678), oxidized CaMKII (methionine 281/282 oxidation, GTX36254), Ryanodine Receptor 2 (RyR2, Millipore, AB9080), RyR2-Ser2814 (badrilla, A010-31), anti-xanthine oxidase (XO, ab109235), anti-NOX4 (ab133303), anti-transforming growth factor-β1 (TGF-β1, ab190503), anti-NOXA2/p67-phox (NOX2, ab109366), and anti-Cytochrome b245 Light Chain/p22-phox (ab75941, Abcam, Cambridge, UK). The membranes were then rinsed with TBST (TBS containing 0.5% Tween-20) and incubated with the above antibodies at a 1:1000 ratio in 0.5% BSA overnight at 4 °C. The secondary antibody was diluted with 5% BSA-TBST: goat anti-rabbit and goat anti-mouse IgG (H + L) HRP 1:10,000, incubated for 40 min at room temperature. After washing three times with TBST, the bands were visualized using the enhanced chemiluminescence (ECL) detection system (GE Healthcare). Finally, ImageJ software was used to analyze the gel images.

2.9. Statistical and bioinformatics analysis

SPSS (version 22.0) was used for all statistical analysis. Normally distributed variables were compared using Student's t-test, or one-way analysis of variance (ANOVA) for multiple comparisons, and the Mann–Whitney rank-sum test was employed for non-normal distributed data, and Chi-square test was used to analyze the counting data. A value of $P < 0.05$ was considered statistically significant. Origin 6.1 and GraphPad Prism 6 were used for data processing and mapping. To identify biological functions, Gene Ontology (GO) annotation [39], DAVID Bioinformatics Resources [40], and STRING software [41] were employed.

Table 1
ECG parameters in ibrutinib-treated mice.

	Control group (n = 6)	Ibrutinib group (n = 6)	P-value (Control VS Ibrutinib)
BW(g)	25.21 ± 1.11	21.09 ± 0.91	7.0419E-8*
HR (bpm)	462.55 ± 74.62	501.33 ± 49.05	0.211
RR (ms)	102.78 ± 2.11	101.03 ± 1.71	0.189
PR (ms)	37.14 ± 0.89	36.08 ± 1.03	0.120
QRS (ms)	9.01 ± 0.12	9.23 ± 0.21	0.087

BW, body weight; HR, heart rate; *P < 0.05.

3. Results

3.1. Ibrutinib enhances AF susceptibility

To verify whether ibrutinib promotes AF, we performed programmed electrical stimulation and obtained ECG recordings. The ECG parameters were unaltered in ibrutinib-treated mice (Table 1, Fig. 1A, C). The results revealed a higher AF incidence in the ibrutinib-treated mice compared with control group (Fig. 1B), and the difference was statistically significant. The duration of burst-pacing-induced AF in ibrutinib-treated mice was significantly longer than that in the control group (Fig. 1D). The parameters of cardiac structure were measured by echocardiography (Fig. 1E–H). These results revealed that the LA diameter of mice in the ibrutinib group was greater than that of control mice, but this difference was not statistically significant (Fig. 1I). The LA area in the ibrutinib group was significantly higher than that in the control group (Fig. 1J). There was no significant difference in LVIDs between the two groups (Fig. 1K). In addition, the E/A peak in the ibrutinib group was significantly lower than that in the control group (Fig. 1L).

3.2. Ibrutinib promotes electrical remodeling by abnormal sarcoplasmic reticulum (SR) Ca^{2+} release

To study the effect of ibrutinib on atrial electrophysiology, we assessed calcium ion release and the SR Ca^{2+} release in atrial cardiomyocytes using IonOptix (Fig. 2A and B). The results showed that spontaneous calcium waves were successfully induced at an extracellular calcium concentration of 2 mM. The atrial myocytes of the ibrutinib group showed a high incidence of spontaneous calcium wave, while the induction success rate of spontaneous calcium waves in the control group was significantly lower (Fig. 2C). Additionally, this study measured the amplitude, decay time, and time to peak of transient calcium changes. Our results indicated that the amplitude of calcium release in atrial myocytes from the ibrutinib group was significantly decreased compared to that of the control group (Fig. 2D). In the ibrutinib group, the decay time of intracellular transient calcium in atrial myocytes was increased (Fig. 2E), while the time to peak of calcium release in the atrial myocytes was decreased, but not significantly (Fig. 2F). Meanwhile, we used the amplitude caffeine-induced Ca^{2+} release to assess SR Ca^{2+} content. The result showed that the amplitude of caffeine-induced Ca^{2+} release slightly reduced in the ibrutinib group than the control group (Fig. 2G), but not statistically significant.

We also assessed the changes in intracellular Ca^{2+} homeostasis in atrial myocytes through confocal imaging (Fig. 2H). The frequency of spontaneous Ca^{2+} spark was significantly increased in ibrutinib group mice (Fig. 2I). Spark duration (FDHM, ms) and spark width (FWHD, um) (Fig. 2J–K), were similar in both groups, but not significantly.

By measuring the intensity of MitoSOX Red staining, we estimated the mitochondrial ROS levels in atrial myocytes (Fig. 2L–M). Our results

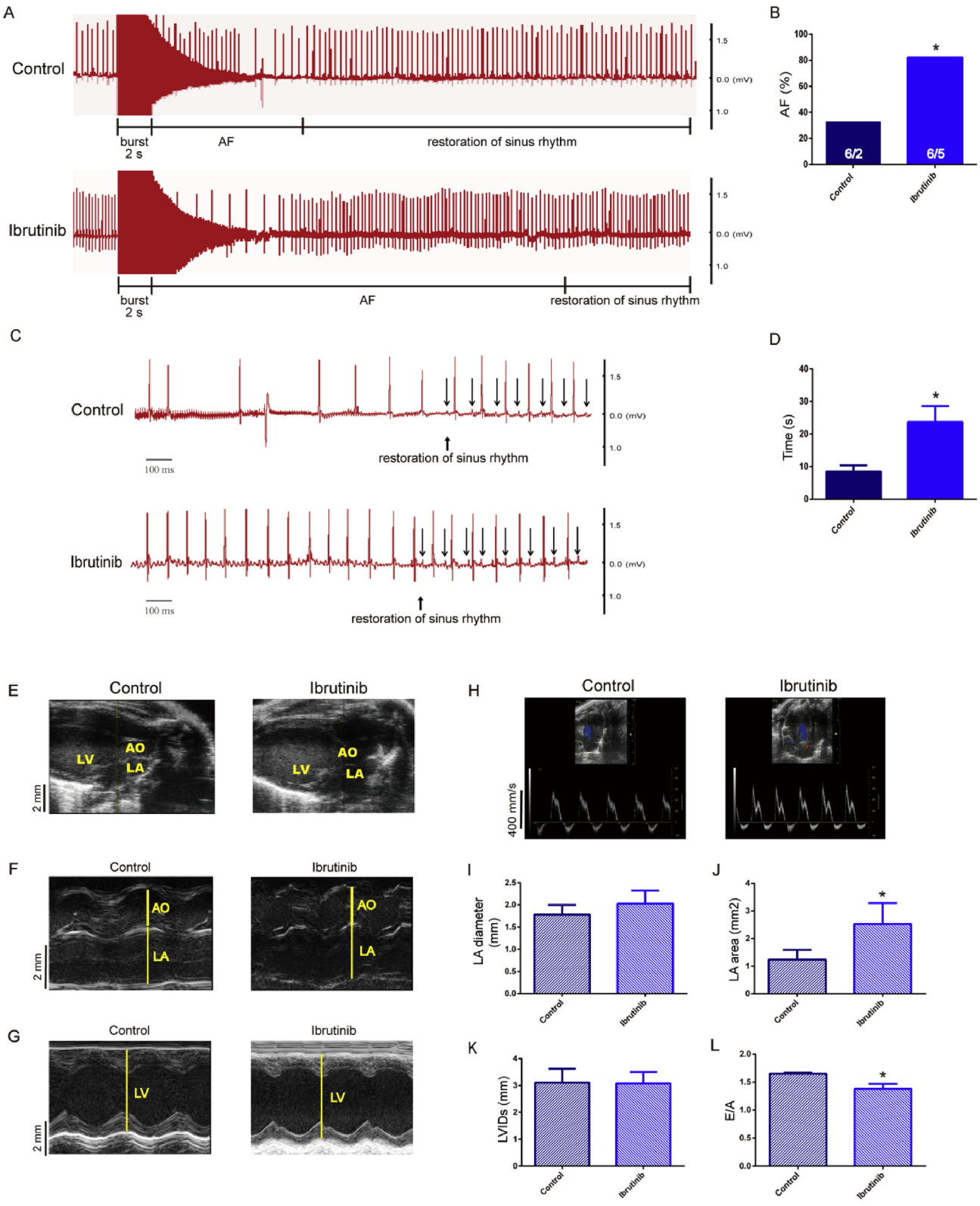

Fig. 1. (A–D) Representative simultaneous recordings of surface ECG in ibrutinib-treated mice and control mice following programmed intracardiac stimulation (n = 6 mice per group; Fig. 1B, Chi-square test; Fig. 1A, C, D, Student's t-test). AF, atrial fibrillation. (E–H) Representative B-mode and M-mode echocardiography recordings and (I–L) quantification of left atrial (LA) diameter, LA area, left ventricular internal dimension systole (LVIDs) and E/A peak in control and ibrutinib-treated mice (n = 4 mice per group; Student's t-test). Values are presented as mean ± SD. *P < 0.05, **P < 0.01 vs Control group.

showed that in the ibrutinib group, after 2 h, mitochondrial ROS production in atrial myocytes was increased by approximately twofold compared to that in the control group, and DTT can reduce the production of ROS.

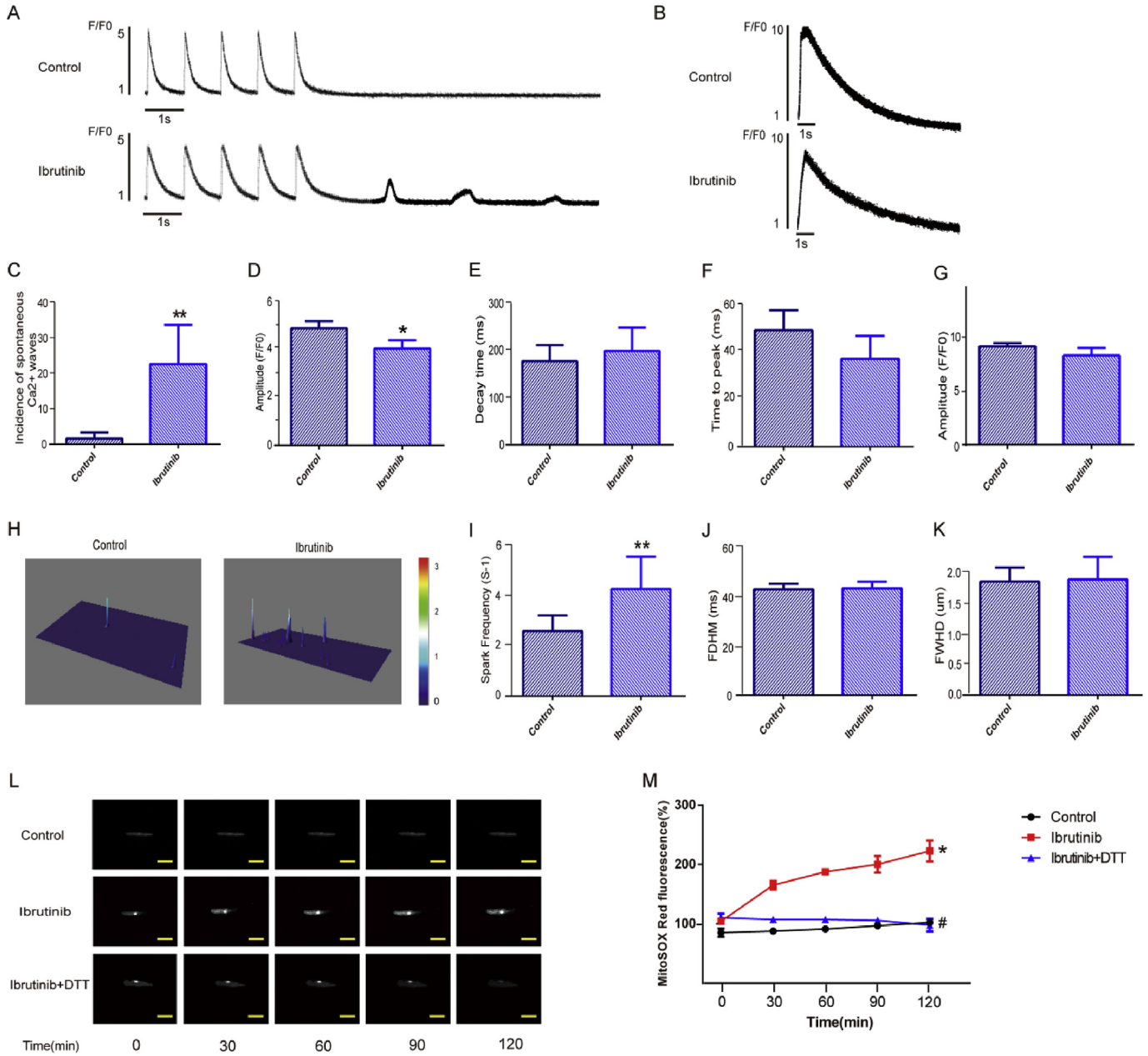

Fig. 2. Ibrutinib promotes electrical remodeling associated with atrial fibrillation (AF) development. (A–B) Representative recordings of transient Ca^{2+} changes (n = 10 cells per group, Student's t-test) and the sarcoplasmic reticulum (SR) Ca^{2+} content (n = 5 cells per group, Student's t-test). (C–G) Quantification of the amplitude, decay time, time to peak of calcium release, and the amplitude of caffeine-induced Ca^{2+} release between the control and ibrutinib-treated groups (n = 10 cells per group; Student's t-test). (H–K) Representative line-scan confocal images and the quantification of Ca^{2+} sparks (CaSF) in control group mice and ibrutinib group mice (n = 10 cells per group; Student's t-test). FDHM, spark duration; FWHD, spark width. (L) Representative images showing the MitoSOX fluorescence intensity in a single atrial myocyte at different times (n = 5 cells per group). Scale bar: 50 μm. (M) Quantification of mitochondrial reactive oxygen species (ROS) production in the control group, ibrutinib group, and DL-Dithiothreitol (DTT) group (n = 5 cells per group; one way ANOVA). Values are presented as mean ± SD. *P < 0.05, **P < 0.01 vs Control group.

3.3. Ibrutinib promotes structural remodeling through fibrosis

To elucidate whether ibrutinib would also promote structural remodeling, we assessed changes in the atrial pathology (Fig. 3). The stained sections photographed and morphologically analyzed at 40 × magnification. The results of masson's trichrome staining indicated that compared to the control group, the ibrutinib group showed myocardial fibrosis and collagen deposition, and that the fibrotic area of mice in the ibrutinib group was significantly greater than that of control mice (Fig. 3A and C). Polarized light microscopy indicated that the myocardial collagen fibers were tightly arranged, and were observed as bright orange-red or yellow. Subsequently, the area of myocardial collagen fibers was compared between the two groups, and it was significantly different (Fig. 3B and D).

Transmission electron microscopy showed the changes in the ultrastructure of mitochondria. In the control group, atrial myocytes showed complete and clear sarcomeres, a neat and tight arrangement of myofilaments, a basically normal mitochondrial structure, and a tight arrangement of ridge. In contrast, in the ibrutinib group, myocardial cells were partially disappeared, and mitochondrial swelling and became deformed, and mitochondrial ridge broke (Fig. 3E). The area of mitochondrial damage in the ibrutinib group was significantly higher

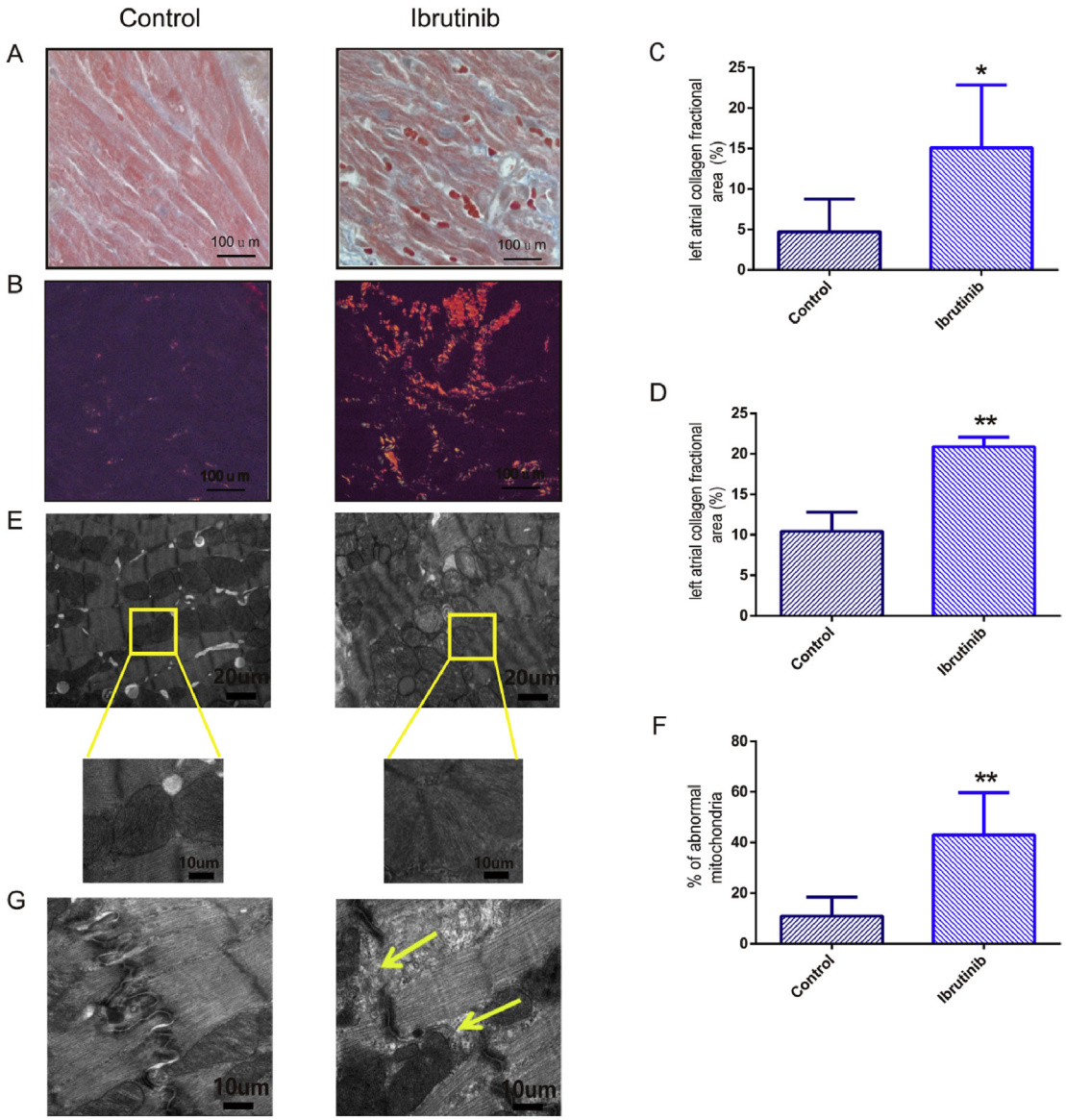

Fig. 3. Ibrutinib promotes structural remodeling associated with AF development. (A) Masson's trichrome staining (40 ×), (B) Sirius red staining (40 ×), (C) quantification of atrial fibrosis (blue) and (D) quantification of type I collagen deposition (red or yellow) in the atria of control and ibrutinib-treated mice. (E) Ultrastructure showed the changes of atrial muscle mitochondria and (F) quantification of mitochondrial damage are in the control group and ibrutinib group. (n = 3 mice per group; Student's t-test) (G) Ultrastructure showed the changes of atrial muscle leap disc in the control group and ibrutinib group (n = 3 mice per group; Student's t-test). Scale bar for A–B: 100 μm; for E: 20 μm; for G: 10 μm. Values are presented as mean ± SD. *P < 0.05, **P < 0.01 vs Control group. (For interpretation of the references to colour in this figure legend, the reader is referred to the Web version of this article.)

than that in the control group (Fig. 3F). Cells in the ibrutinib group also showed signs of cleavage of the gap junctions, expanded T tube, and flocculation or myeloid secretions in the gap junctions (Fig. 3G).

3.4. Proteomics analysis of ibrutinib-induced AF mice atrial tissue

Isobaric tagging for relative and absolute quantitation (iTRAQ) based on proteomics explicitly authenticated and quantified a total of 2675 proteins. The FC values and the significant differences between each group were calculated by Student's t-test, and the significantly differentially expressed proteins were screened with cutoff values of $0.67 > FC > 1.2$ and $P < 0.05$. Fig. 4A shows a volcano map of the differentially expressed proteins. In addition, the specific combinations of differentially expressed proteins within each group were compared to obtain 184 dynamically changing proteins to better explain the expression patterns of these proteins under different treatments.

A total of 184 proteins were differentially expressed between the control and ibrutinib groups; these were used for further statistical analysis (Table S1). The OmicsBean omics data integration analysis platform was used to perform functional annotation and enrichment analysis of the genes encoding the differentially expressed proteins through GO. GO functional annotations include three levels of analysis: biological process, cellular component, and molecular function. We chose to explore molecular function (Fig. 4B) and the KEGG pathway (Fig. 4C) corresponding to the major proteins in molecular function. In order to further analyze the functional characteristics of the differentially expressed proteins, we chose to validate the proteins in Fig. 4C. An expression pattern clustering heat map analysis was performed using R language. In the clustering heat map, which included 23 proteins, major clusters could be observed, including the up- and down-regulation of proteins (Fig. 4D, Table 2). Meanwhile, protein-protein interaction (PPI) network analysis indicated differentially expressed proteins related to ROS production (Fig. 4E). These differentially expressed proteins were therefore shown to be associated with ROS-

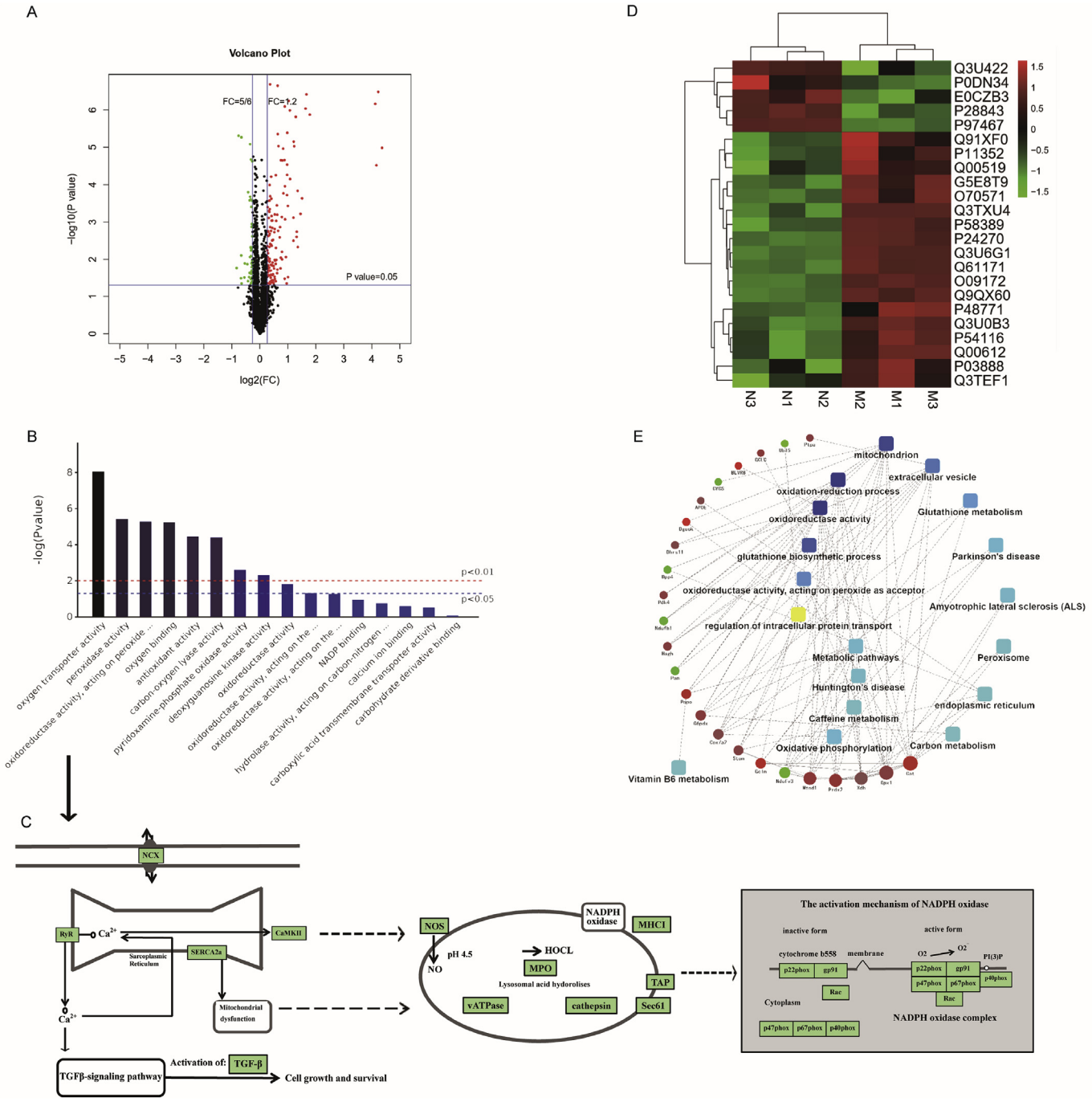

Fig. 4. Identification and quantitative analysis of differentially expressed atrial tissue proteins in the control group vs. the ibrutinib group. (A) Differential protein expression was verified using Student's t-test and a volcano plot was constructed. (B) Gene Ontology (GO) annotation and enrichment of differentially expressed proteins. (C) KEGG Pathway analysis. (D) The clustering heat map analysis. (E) Protein-protein interaction (PPI) network showing twenty-three major nodes. n = 3 mice per group. NCX, calcium and sodium exchangers; RyR2, Ryanodine Receptor 2; CaMKII, Ca^{2+}/calmodulin-dependent protein kinase II; TGF-β, transforming growth factor-β; NOS, nitric oxide synthase; NADPH oxidase, nicotinamide adenine dinucleotide phosphate oxidase; MPO, myeloperoxidase; HOCL, hypochlorous; MHCI, MHC class I molecule.

related pathways; this requires further validation.

3.5. Selection and verification of proteins by Western blot analysis in ibrutinib-induced AF mice

To choose proteins for verification, we reviewed the results of bioinformatics analysis of the proteins to determine differential protein expression. Among the proteins of interest, oxidative stress-related proteins have been previously reported to be associated with AF, and NOX is a major source of increased ROS in AF [42]. Thus, we selected five ROS-related proteins, NOX2, NOX4, p22-phox, XO, and TGF-β, and treated mice with the NOX inhibitor apocynin for verification. The abundance of the analyzed proteins was detected by western blotting (Fig. 5).

The results indicated that the protein expression of NOX2 in the ibrutinib group was significantly increased compared to that in the control group, while the protein expression of NOX2 in the apocynin group was significantly lower than that in the ibrutinib group (Fig. 5A).

Table 2
Atrial proteins change during the course of ibrutinib-treated mice.

Accession	Protein description	FC	p value
Q3U422	NADH dehydrogenase [ubiquinone] flavoprotein 3, mitochondrial	0.764989455	0.030646246
P0DN34	NADH dehydrogenase [ubiquinone] 1 beta subcomplex subunit 1	0.809436275	0.02431271
E0CZB3	Ubiquitin-like protein 5	0.733027523	0.013441889
P28843	Dipeptidyl peptidase 4	0.8166717	0.001348482
P97467	Peptidyl-glycine alpha-amidating monooxygenase	0.828167319	2.39669E-05
Q91XF0	Pyridoxine-5′-phosphate oxidase	1.66263048	0.017499651
P11352	Glutathione peroxidase 1	1.34082535	0.014289449
Q00519	Xanthine dehydrogenase/oxidase	1.209218581	0.028863429
G5E8T9	Hydroxyacyl glutathione hydrolase	1.356819894	0.033973033
O70571	[Pyruvate dehydrogenase (acetyl-transferring)] kinase isozyme 4, mitochondrial	1.354865424	0.003127967
Q3TXU4	Apolipoprotein E	1.249906191	0.000506787
P58389	Serine/threonine-protein phosphatase 2A activator	1.337628866	0.00091491
P24270	Catalase	1.683681672	2.22357E-05
Q3U6G1	Biliverdin reductase B (Flavin reductase (NADPH))	1.841543514	2.20116E-05
Q61171	Peroxiredoxin-2	1.483031674	5.59178E-05
O09172	Glutamate–cysteine ligase regulatory subunit	1.744881245	2.25555E-05
Q9QX60	Deoxyguanosine kinase, mitochondrial	1.961555457	5.48505E-05
P48771	Cytochrome *c* oxidase subunit 7A2, mitochondrial	1.26056584	0.016824736
Q3U0B3	Dehydrogenase/reductase SDR family member 11	1.276419842	0.000454448
P54116	Erythrocyte band 7 integral membrane protein	1.320867614	0.004096078
Q00612	Glucose-6-phosphate 1-dehydrogenase X	1.382615444	0.003007136
P03888	NADH-ubiquinone oxidoreductase chain 1	1.437668854	0.029811979
Q3TEF1	Glutamate–cysteine ligase catalytic subunit	1.402177858	0.043943686

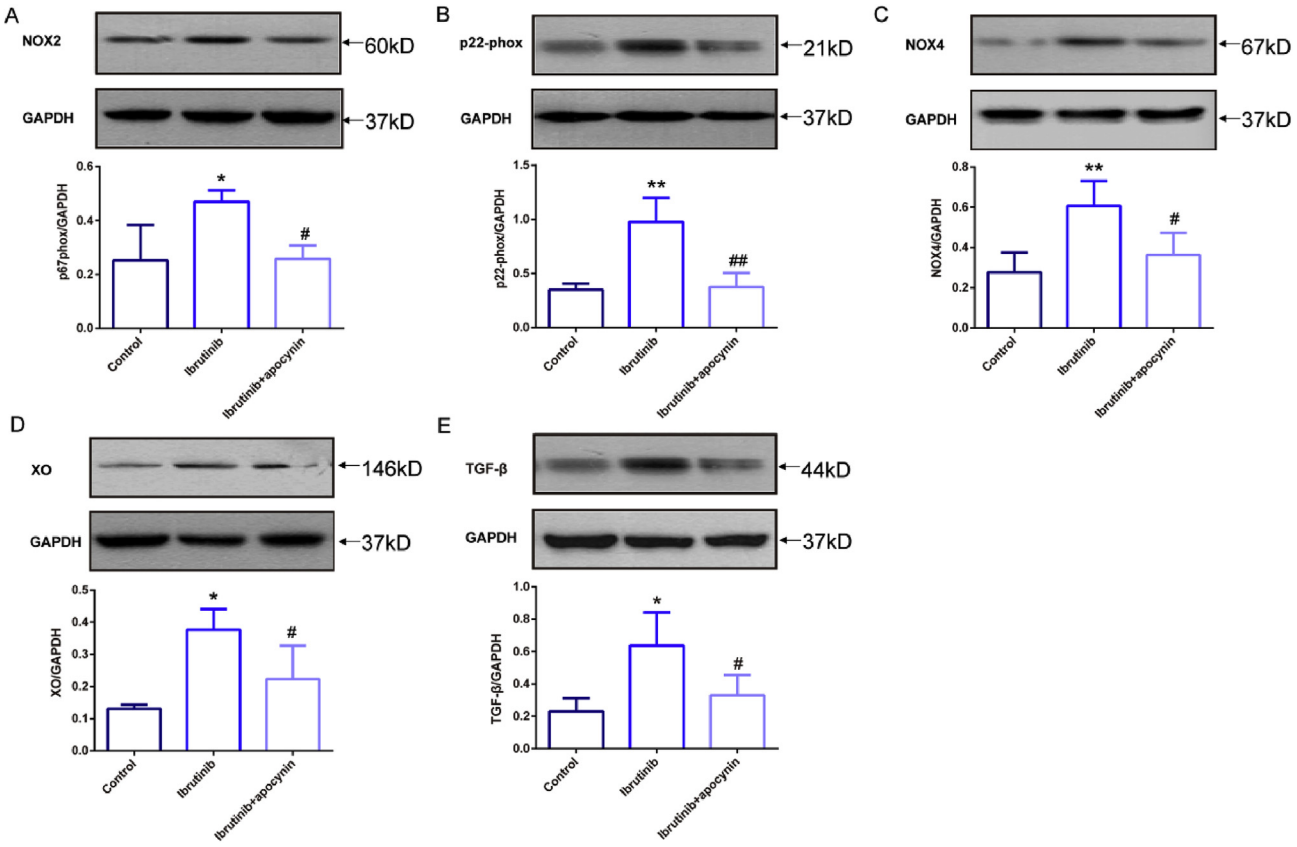

Fig. 5. Enhanced activation of oxidative stress-related signaling pathways in ibrutinib-treated mice. (A–E) Representative western blots and quantification of anti-NOXA2/p67-phox (NOX2), anti-Cytochrome b245 Light Chain/p22-phox (p22-phox), NOX4, anti-xanthine oxidase (XO), and anti-transforming growth factor-β1 (TGF-β1) expression in the atrial tissues of AF mice in the control group, ibrutinib group, and apocynin group with GAPDH as a loading control (n = 3 mice per group; one way ANOVA). Values are presented as mean ± SD. $^{*}P < 0.05$, $^{**}P < 0.01$ vs Control group. $\#p < 0.05$, $\#\#p < 0.01$ vs. Ibrutinib group.

The p22-phox protein expression in the ibrutinib group was significantly higher than that in the control group, but that in the apocynin group was significantly lower than that in the ibrutinib group (Fig. 5B). The protein expression of NOX4 in the ibrutinib group was significantly higher than that in the control group, and was significantly reduced after treatment with apocynin (Fig. 5C). In addition, XO protein expression in the ibrutinib group was significantly higher than that in the control group, but was decreased in the apocynin group compared to that in the ibrutinib group (Fig. 5D). TGF-β protein expression in the ibrutinib group was significantly increased compared to that in the

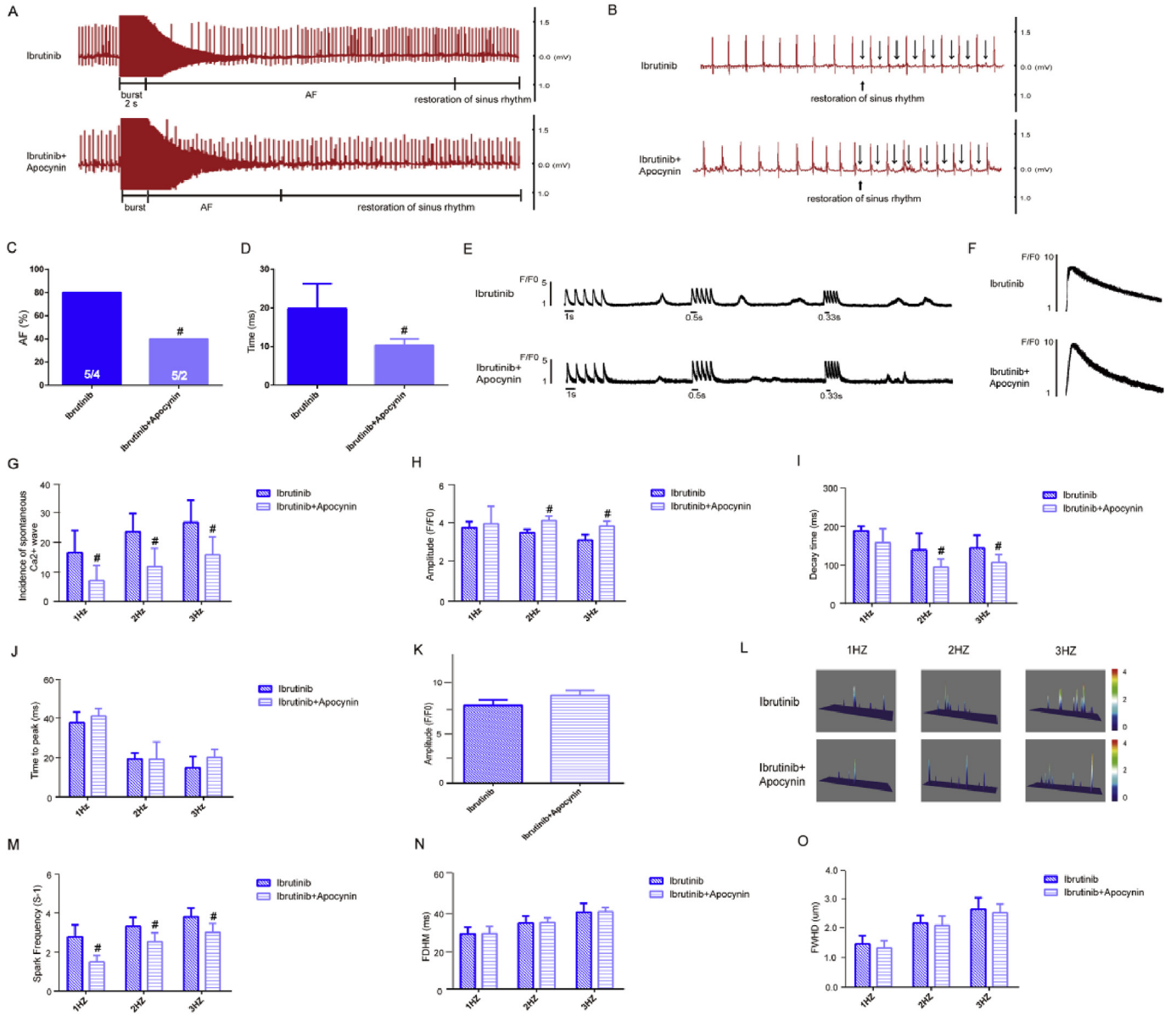

Fig. 6. Apocynin inhibits electrical remodeling in ibrutinib promotes atrial fibrillation (AF). (A–D) The incidence and duration of burst-pacing-induced AF in mice from the ibrutinib group and apocynin group (n = 5 mice per group; Fig. 6C, Chi-square test; Fig. 6D, Student's t-test). (E–F) Representative recordings of transient Ca^{2+} release (n = 6 cells per group, Student's t-test) and sarcoplasmic reticulum (SR) Ca^{2+} content (n = 3 cells per group, Student's t-test). (G–K) Quantification of amplitude, decay time, time to peak of transient Ca^{2+}, and the amplitude of caffeine-induced Ca^{2+} release in the ibrutinib group and apocynin group; (n = 6 cells per group, Student's t-test). (L–O) Representative line-scan confocal images and the quantification of Ca^{2+} sparks (CaSF) in ibrutinib group mice and apocynin group mice (n = 5 cells per group, Student's t-test). FDHM, spark duration; FWHD, spark width. Values are presented as mean ± SD. #p < 0.05, ##p < 0.01 vs. Ibrutinib group.

control group, and this increase was reversed in the apocynin group (Fig. 5E).

3.6. Inhibition of NOX reduced AF inducibility

To determine whether the inhibition of NOX would reduce the duration of AF and prevent abnormal SR Ca^{2+} release in ibrutinib-treated mice, we performed ECG (Fig. 6A–B) and calcium ion release measurements (Fig. 6E–F). ECG measurements showed that the AF duration and incidence in the apocynin group was obviously reduced compared to that in the ibrutinib group (Fig. 6C–D). Spontaneous Ca^{2+} waves and SR Ca^{2+} release were recorded at 1 Hz–3Hz in the ibrutinib group and apocynin group (Fig. 6E–F). The results showed that the spontaneous calcium wave incidence in the apocynin group was significantly reduced compared to that in the ibrutinib group (Fig. 6G).

Next, we measured the time to peak, amplitude, and decay time of transient calcium. The results at 1 Hz stimulation showed that there was no statistical difference in the calcium release amplitude of the apocynin group compared with that of the ibrutinib group. However, at 2 Hz and 3 Hz indicated that the amplitude of calcium release in the apocynin group was significantly increased compared to that in the ibrutinib group (Fig. 6H). At 1 Hz–3Hz stimulation, the delay time of transient Ca^{2+} in atrial myocytes from the apocynin group was obviously decreased compared to that in the ibrutinib group (Fig. 6I). But the time to peak of transient Ca^{2+} in the apocynin group was higher than that in the ibrutinib group; however, there were no significant differences between the two groups (Fig. 6J). Meanwhile, the amplitude of caffeine-induced Ca^{2+} release slightly increased in the apocynin group

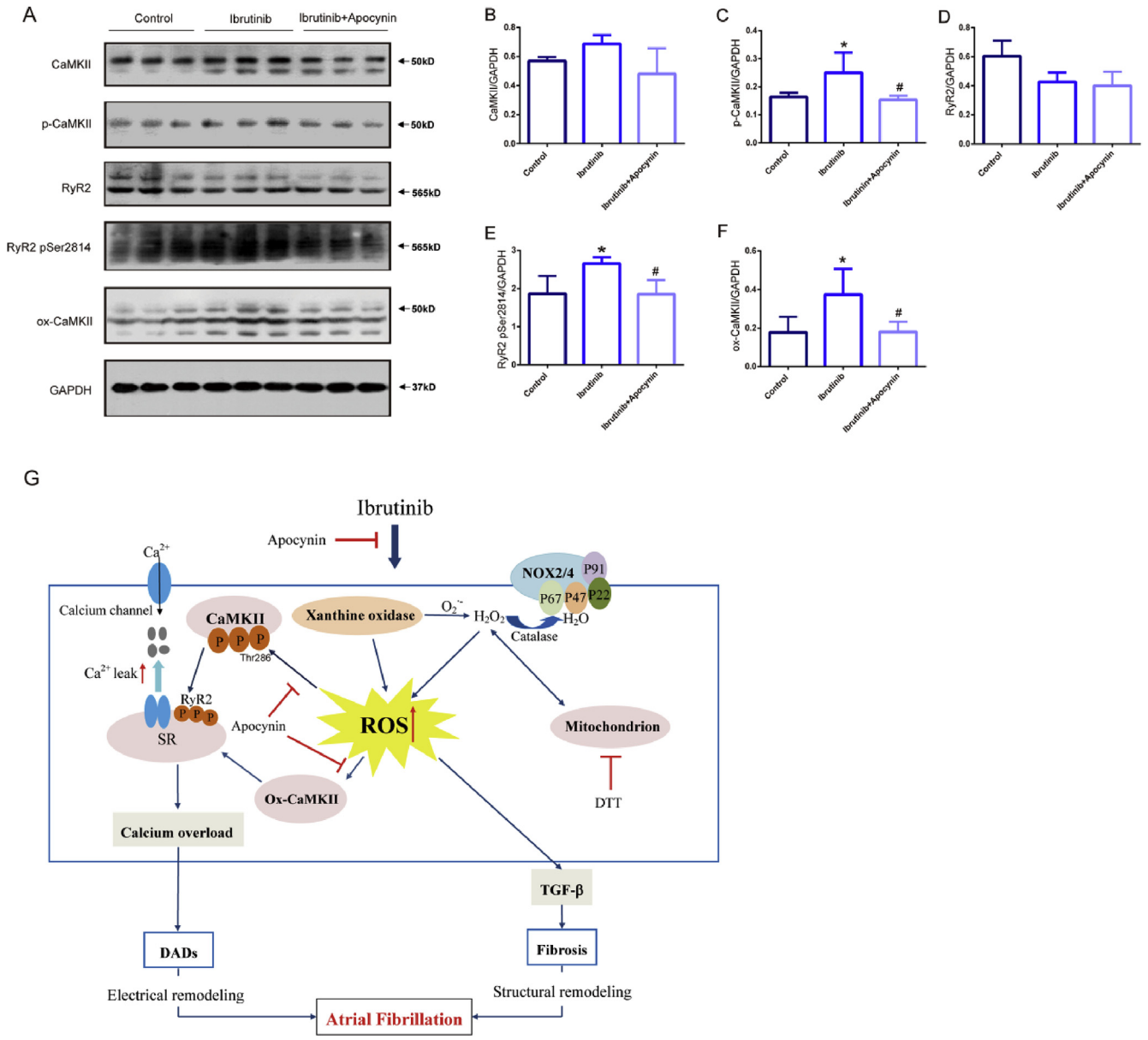

Fig. 7. Reactive oxygen species (ROS) activates oxidized Ca^{2+}/calmodulin-dependent protein kinase II (ox-CaMKII) increasing serine 2814 on RyR2, and the inhibitory effect of apocynin. (A–F) Representative western blots and quantification of anti-calmodulin-dependent protein kinases II (CaMKII), anti-CaMKII (phospho T286, *p*-CaMKII), oxidized CaMKII, Ryanodine Receptor 2 (RyR2), RyR2-Ser2814 expression in the atrial tissues of mice in the control group, ibrutinib group, and apocynin group with GAPDH as a loading control (n = 3 mice per group, one way ANOVA). Values are presented as mean ± SD. $^{*}P < 0.05$, $^{**}P < 0.01$ vs Control group. $\#p < 0.05$, $\#\#p < 0.01$ vs. Ibrutinib group. (G) Working model of AF-promoting mechanisms due to ibrutinib. SR, sarcoplasmic reticulum; ROS, reactive oxygen species; RyR2, Ryanodine Receptor 2; CaMKII, Ca^{2+}/calmodulin-dependent protein kinase II; ox-CaMKII, oxidized CaMKII; DTT, DL-Dithiothreitol; DADs, delayed afterdepolarizations; TGF-β, transforming growth factor-β.

than the ibrutinib group (Fig. 6K), but not statistically significant.

Furthermore, spontaneous Ca^{2+} spark were also recorded at 1 Hz–3Hz in the ibrutinib group and apocynin group (Fig. 6L). The results at 1 Hz–3Hz stimulation indicated that the frequency of spontaneous Ca^{2+} spark in the apocynin group was markedly lower than in the ibrutinib group, and the difference was statistically significant (Fig. 6M). Upon 1 Hz–3Hz stimulation, compared to that in the ibrutinib group, the spark duration and spark width of the apocynin group was reduced, but not statistically significant (Fig. 6N–O).

3.7. NADPH oxidase and CaMKII pathway

NADPH oxidase–dependent ROS and elevated ox-CaMKII are critical for the proarrhythmic actions in pacing-induced AF [42] and that targeted antioxidant therapy, apocynin, can reduce or prevent AF in ibrutinib–treated mice. We evaluated the expression of ox-CaMKII in ibrutinib-treated atrial myocytes and the inhibitory effect of apocynin. The results showed that the total levels of CaMKII and RyR2 were not obviously increased. However, ibrutinib group significantly increased the expression of ox-CaMKII, *p*-CaMKII (Thr-286) and *p*-RyR2 (Ser2814), and apocynin reduced the expression of these proteins (Fig. 7A and B).

4. Discussion

In this study, we found that increased ROS activity in ibrutinib-treated mice promoted the production of AF-maintaining substrates that ultimately increased their susceptibility to AF. Ibrutinib treatment

activates NOX to increase ROS, resulting in oxidation of methionines 281/282 in Ca^{2+}/calmodulin-dependent protein kinase II (ox-CaMKII) increasing serine 2814 on RyR2, causing enhanced diastolic Ca^{2+} leak that promotes electrical and structural remodeling. Apocynin, an inhibitor of NOX, reduced the development of AF and atrial remodeling. These results provide new pathophysiological insights into and potential treatments for ibrutinib-induced AF promotion.

Previous studies have raised the valid concern that ibrutinib may increase the risk of AF; accumulating evidence indicates that ibrutinib-induced AF promotion is the most common side-effect of this treatment [10,43,44]; although individual studies have varied in the extent to which they observed these adverse events [3,4,6,45]. To explore the mechanisms of AF contributing to this outcome, this study used iTRAQ-based quantitative proteomics to analyze the changes in protein expression after burst-pacing-induced AF in ibrutinib-treated mice, and screened the differentially expressed proteins for GO function annotation and clustering heat map analysis, and then constructed a PPI network. The screened differential proteins included NADH dehydrogenase [ubiquinone] flavoprotein 3, glutathione peroxidase 1, xanthine dehydrogenase/oxidase, and peroxiredoxin-2, among others. Elevated levels of these proteins can promote the development of AF, and these differentially expressed proteins were found to be closely related to oxidative stress-related signaling pathways.

Our proposed model of the ROS-mediated ibrutinib-treated mice mechanism of AF development is multifactorial (Fig. 7C) ROS enhances the expression of ox-CaMKII, leading to RyR2 serine 2814 mediated SR Ca^{2+} release events [17,46–48] which ultimately cause the generation of AF. Our results demonstrated that ibrutinib increased SR Ca^{2+} release events, particularly the spontaneous calcium wave, the amplitude of transient calcium signals, the decay time, and the frequency of calcium sparks, all of which can provide a substrate for AF development. Mitochondrial ROS production was increased by more than two-fold after the infiltration of atrial myocytes in ibrutinib-treated mice. The use of the inhibitor DTT reduced ibrutinib-treated mitochondrial ROS production, improved calcium regulation disorder in atrial myocytes, and reduced spontaneous calcium release from the SR. Increasing evidence indicates that abnormal calcium in atrial myocytes is an important factor leading to the progression and maintenance of AF [49–53]. During atrial fibrillation, the calcium leakage of RyR from the SR is increased. By regulating the expression of ion channels and intracellular calcium homeostasis, transient calcium changes in myocardial cells are increased to promote further atrial electrical remodeling [54,55]. Thus, these results support the function of ROS in triggering abnormal calcium release, leading to electrical remodeling in ibrutinib-treated AF mice.

During the development of cardiac arrhythmias, myocardial fibrosis plays a vital role in up-regulating the expression of the necessary substrates for the persistence of these arrhythmias [58]. Under pathological conditions associated with the development of fibrosis in patients with AF, the structure of fibrotic myocardium tissue becomes uneven, thus affecting intercellular conduction [56–58] and resulting in slowed conduction, as well as functional and structural blockage, thereby producing AF-related substrates [59]. Therefore, we evaluated the changes in atrial size and area through echocardiography, and used histopathological staining to ascertain the degree of myocardial fibrosis. In our mouse model of burst-pacing-induced AF, the LA diameter, and LA area were increased by treatment with ibrutinib. Light microscopy showed an increase in myocardial cell production and a wider cell gap, as well as a slight increase in collagen fibers. Transmission electron microscopy showed changes in the myocardial ultrastructure, including decreased sarcomeres and SR, mitochondrial swelling, and glycogen deposition. Furthermore, TGF-β has been shown to participate in the development of atrial fibrosis [60–62] by activating ROS; redox-sensitive signaling pathways are known to regulate TGF-β-induced myocardial structural remodeling [63,64]. The results of this study indicated that the expression of TGF-β was clearly increased in ibrutinib-treated mice. Serum TGF-β levels have been found to be increased in AF patients receiving defibrillation treatment [62]. Furthermore, TGF-β over-expression has caused substantial increases in atrial fibrosis, affected conduction characteristics, and induced the development of AF [61,65].

Antioxidant treatment has been shown to have some preventive functions against post-operative AF [66,67], and against the occurrence and development of AF [68,69]. Apocynin, which is an extract of several plants, is an inhibitor of NOX [70]; it acts by inhibiting the active site of NOX [71]. Studies have shown that apocynin may be effective against AF, as its anti-oxidative action may also regulate the related stimulation of atrial remodeling. Nevertheless, antioxidants as upstream therapies may interact more effectively with target proteins prior to ROS production [72]. As a valid inhibitor of NOX, apocynin can pre-emptively prevent the formation of ROS. Our study demonstrates that apocynin markedly down-regulated the expression of atrial proteins, including NOX2, Nox4, p22-phox, XO and TGF-β, and also blocked the development of AF by regulating the expression of oxidative stress-related proteins. As an inhibitor of NOX, it can also reduce ROS production through the rapid electrical stimulation of atrial myocytes [73]. It has been shown in basic experimental studies and clinical trials that ROS in atrial tissue participates in atrial remodeling, and that ROS plays a key role in atrial fibrosis [42,74–76]. Hence, inhibiting ROS may be a target for the management of AF. Our study showed that apocynin inhibited the increase in SR Ca^{2+} release events to attenuate atrial electrical remodeling and to reduce the induction and duration of AF [77].

CaMKII and increased ROS pathway are now recognized to contribute to cardiac arrhythmias [47,78,79]. Multiple studies have validated *p*-RyR2(Ser2814) as a CaMKII phosphorylation target, and that hyperphosphorylation of Ser2814 promotes diastolic SR Ca^{2+} release and pacing-induced AF [48,80,81]. Under increased oxidative stress, CaMKII is activated by oxidation of methionines (methionines 281/282) [17], suggesting a possible role for ox-CaMKII as an ROS-activated proarrhythmic signal in AF [47]. Another recent study showed that oxidized CaMKII was increased in atria from patients with AF compared to patients in sinus rhythm. In a rapid pacing model of inducible AF, mice expressing a CaMKII-resistant RyR, due to knock-in mutation of a CaMKII phosphorylation site, also had reduced susceptibility to AF induction in the model, further supporting the idea that oxidized CaMKII is inducing AF via RyR phosphorylation [48]. Other studies have shown that oxidative stress can activate p-calmodulin kinase, thereby promoting the release of calcium in the SR and causing arrhythmias [82]. In the present study, our results indicated that ibrutinib group increased the protein expression of ox-CaMKII, *p*-RyR2(Ser2814) and *p*-CaMKII (Ser286), and apocynin reduced these proteins expression. Taken together, these findings suggest that ROS and elevated ox-CaMKII and *p*-CaMKII(Ser286) are critical for the actions of ibrutinib in pacing-induced AF and that apocynin reduced the ox-CaMKII protein and *p*-CaMKII(Ser286)expression to relieve the SR Ca^{2+} release events, thus reducing or preventing AF in ibrutinib–treated mice. However, due to the small sample size, this result still needs further research to prove.

Some limitations should be acknowledged. Firstly, while ibrutinib may have promoted cardiac remodeling in the atria, it may also have had an effect on ventricular remodeling; this needs to be verified in further studies. Secondly, although our data revealed that ROS activity was enhanced in ibrutinib-treated mice, the detailed upstream factors leading to the activation of ROS production were not investigated in the current study. Thirdly, the AF duration in our study was significantly longer than in previous studies [81,83–85]. It may be that different types of stimulation electrodes and different stimulation intensities lead to different duration of AF. Finally, although apocynin effectively reduced AF inducibility in ibrutinib-treated mice, we did not determine the precise pharmacokinetics of apocynin or its potential adverse effects on cardiac function. Further studies are needed to solve these issues.

In summary, our study showed that ROS production in atrial

cardiomyocytes was associated with the pathogenesis of ibrutinib promoted AF. Oxidative stress induction in ibrutinib-treated mice caused calcium overload and atrial fibrosis by increasing ox-CaMKII, *p*-CaMKII (Ser286) and *p*-RyR2(Ser2814) TGF-β expression, which is associated with atrial remodeling. Apocynin, an inhibitor of NOX, attenuated atrial remodeling in ibrutinib-treated mice by inhibiting the expression of oxidative stress-related proteins, ox-CaMKII and *p*-CaMKII(Ser286). That the findings of this study can potentially open up new clinical mechanism-based targets to prevent and treat ibrutinib promoted AF.

Declaration of competing interest

The authors state no potential conflict of interest.

Acknowledgements

The work was supported by the National Natural Science Foundation of China (Grant No. 81430098, 81870244, and 81725024), the National Key Research and Development Program of China (Grant No.2017YFC1700400 and 2018YFC1704901), National high-level talent special support plan (No.W02020052), the Beijing Natural Science Foundation (No.7152049), and the research project of Beijing University of Chinese Medicine (2019-JYB-XS-136).

Appendix A. Supplementary data

Supplementary data to this article can be found online at https://doi.org/10.1016/j.redox.2020.101432.

References

[1] Fda, Approval for ibrutinib, Accessed: July 2017, 2015. http://www.cancer.gov/aboutcancer/treatment/drugs/fda-ibrutinib.
[2] S. O'Brien, R.R. Furman, S. Coutre, I.W. Flinn, J.A. Burger, K. Blum, J. Sharman, W. Wierda, J. Jones, W. Zhao, N.A. Heerema, A.J. Johnson, Y. Luan, D.F. James, A.D. Chu, J.C. Byrd, Single- agent ibrutinib in treatment- naive and relapsed/refractory chronic lymphocytic leukemia: a 5- year experience, Blood 131 (2018) 1910–1919.
[3] *, J.A. Burger, A. Tedeschi, P.M. Barr, T. Robak, C. Owen, P. Ghia, O. Bairey, P. Hillmen, N.L. Bartlett, J. Li, D. Simpson, S. Grosicki, S. Devereux, H. McCarthy, S. Coutre, H. Quach, G. Gaidano, Z. Maslyak, D.A. Stevens, A. Janssens, F. Offner, J. Mayer, M. O'Dwyer, A. Hellmann, A. Schuh, T. Siddiqi, A. Polliack, C.S. Tam, D. Suri, M. Cheng, F. Clow, L. Styles, D.F. James, T.J. KippsRESONATE-2 Investigators, Ibrutinib as initial therapy for patients with chronic lymphocytic leukemia, N. Engl. J. Med. 373 (2015) 2425–2437.
[4] M. Dreyling, W. Jurczak, M. Jerkeman, R.S. Silva, C. Rusconi, M. Trneny, F. Offner, D. Caballero, C. Joao, M. Witzens-Harig, G. Hess, I. Bence-Bruckler, S. Cho, J. Bothos, J.D. Goldberg, C. Enny, S. Traina, S. Balasubramanian, ... S. Rule, Ibrutinib versus temsirolimus in patients with relapsed or refractory mantle-cell lymphoma: an international, randomised, open-label, phase 3 study, Lancet 387 (2016) 770–778.
[5] T.D. Shanafelt, S.A. Parikh, P.A. Noseworthy, V. Goede, K.G. Chaffee, J. Bahlo, T.G. Call, S.M. Schwager, W. Ding, B. Eichhorst, K. Fischer, J.F. Leis, A.A. Chanan-Khan, M. Hallek, S.L. Slager, N.E. Kay, Arial fibrillation in patients with chronic lymphocytic leukemia (CLL), Leuk. Lymphoma 58 (2017) 1630–1639.
[6] J.C. Byrd, J.R. Brown, S. O'Brien, J.C. Barrientos, N.E. Kay, N.M. Reddy, S. Coutre, C.S. Tam, S.P. Mulligan, U. Jaeger, S. Devereux, P.M. Barr, R.R. Furman, T.J. Kipps, F. Cymbalista, C. Pocock, P. Thornton, F. Caligaris-Cappio, T. Robak, J. Delgado, S.J. Schuster, M. Montillo, A. Schuh, S. de Vos, D. Gill, A. Bloor, C. Dearden, C. Moreno, J.J. Jones, A.D. Chu, M. Fardis, J. McGreivy, F. Clow, D.F. James, P. Hillmen, For the RESONATE Investigators*, Ibrutinib versus ofatumumab in previously treated chronic lymphoid leukemia, N. Engl. J. Med. 371 (2014) 213–223.
[7] D.P. Leong, F. Caron, C. Hillis, A. Duan, J.S. Healey, G. Fraser, D. Siegal, The risk of atrial fibrillation with ibrutinib use: a systematic review and meta-analysis, Blood 128 (2016) 138–140.
[8] X.Y. Yang, X.Y. Li, M.C. Yuan, C. Tian, Y.H. Yang, X.F. Wang, X.Y. Zhang, Y. Sun, T.M. He, S.J. Han, G. Chen, N. Liu, Y.H. Gao, D. Hu, Y.W. Xing, H.C. Shang, Anticancer therapy-induced atrial fibrillation: electrophysiology and related mechanisms, Front. Pharmacol. 9 (2018) 1058.
[9] J.R. Brown, J. Moslehi, S. O'Brien, P. Ghia, P. Hillmen, F. Cymbalista, T.D. Shanafelt, G. Fraser, S. Rule, T.J. Kipps, S. Coutre, M. Dilhuydy, P. Cramer, A. Tedeschi, U. Jaeger, M. Dreyling, J.C. Byrd, A. Howes, M. Todd, J. Vermeulen, D.F. James, F. Clow, L. Styles, R. Valentino, M. Wildgust, M. Mahler, J.A. Burger, Characterization of atrial fibrillation adverse events reported in ibrutinib randomized controlled registration trials, Haematologica 102 (2017) 1796–1805.
[10] T.E. Wiczer, L.B. Levine, J. Brumbaugh, J. Coggins, Q. Zhao, A.S. Ruppert, K. Rogers, A. McCoy, L. Mousa, A. Guha, N.A. Heerema, K. Maddocks, B. Christian, L.A. Andritsos, S. Jaglowski, S. Devine, R. Baiocchi, J. Woyach, J. Jones, M. Grever, K.A. Blum, J.C. Byrd, F.T. Awan, Cumulative incidence, risk factors, and management of atrial fibrillation in patients receiving ibrutinib, Blood Adv. 1 (2017) 1739–1748.
[11] S.S. Chugh, R. Havmoeller, K. Narayanan, D. Singh, M. Rienstra, E.J. Benjamin, R.F. Gillum, Y. Kim, J.H. McAnulty, Z. Zheng, M.H. Forouzanfar, M. Naghavi, G.A. Mensah, M. Ezzati, C.J.L. Murray, Worldwide epidemiology of atrial fibrillation: a global burden of disease 2010 study, Circulation 129 (2014) 837–847.
[12] E.J. Benjamin, P.A. Wolf, R.B. D'Agostino, H. Silbershatz, W.B. Kannel, D. Levy, Impact of atrial fibrillation on the risk of death the Framingham Heart Study, Circulation 98 (1999) 946–952.
[13] P.A. Noseworthy, B.J. Gersh, D.M. Kent, J.P. Piccini, D.L. Packer, N.D. Shah, X. Yao, Atrial fibrillation ablation in practice: assessing CABANA generalizability, Eur. Heart J. 40 (2019) 1257–1264.
[14] K.L. Weeks, X. Gao, X. Du, E.J.H. Boey, A. Matsumoto, B.C. Bernardo, H. Kiriazis, N. Cemerlang, J.W. Tan, Y.K. Tham, T.F. Franke, H. Qian, M.A. Bogoyevitch, E.A. Woodcock, M.A. Febbraio, P. Gregorevic, J.R. McMullen, Phosphoinositide 3-kinase p110alpha is a master regulator of exercise induced cardioprotection and PI3K gene therapy rescues cardiac dysfunction, Circ. Heart Fail. 5 (2012) 523–534.
[15] J.R. McMullen, E.J.H. Boey, J.Y.Y. Ooi, J.F. Seymour, M.J. Keating, C.S. Tam, Ibrutinib increases the risk of atrial fibrillation, potentially through inhibition of cardiac PI3K-Akt signaling, Blood 124 (2014) 3829–3830.
[16] L. Jiang, L. Li, Y. Ruan, S. Zuo, X. Wu, Q. Zhao, Y. Xing, X. Zhao, S. Xia, R. Bai, X. Du, N. Liu, C. Ma, Ibrutinib promotes atrial fibrillation by inducing structural remodeling and calcium dysregulation in the atrium, Heart Rhythm S1547–5271 (2019) 30308-X.
[17] J.R. Erickson, M.A. Joiner, X. Guan, W. Kutschke, J. Yang, C.V. Oddis, R.K. Bartlett, J.S. Lowe, S. O'Donnell, N. Aykin-Burns, M.C. Zimmerman, K. Zimmerman, A.L. Ham, R.M. Weiss, D.R. Spitz, M.A. Shea, R.J. Colbran, P.J. Mohler, M.E. Anderson, A dynamic pathway for calcium-independent activation of CaMKII by methionine oxidation, Cell 133 (2008) 462–474.
[18] P.D. Swaminathan, A. Purohit, S. Soni, N. Voigt, M.V. Singh, A.V. Glukhov, Z. Gao, B.J. He, E.D. Luczak, M.A. Joiner, W. Kutschke, J. Yang, J.K. Donahue, R.M. Weiss, I.M. Grumbach, M. Ogawa, P. Chen, I. Efimov, D. Dobrev, P.J. Mohler, T.J. Hund, M.E. Anderson, Oxidized CaMKII causes cardiac sinus node dysfunction in mice, J. Clin. Investig. 121 (2011) 3277–3288.
[19] J. Palomeque, C.A. Valverde, J.O. Velez Rueda, M.A. Salas, A. Mattiazzi, M. Vila Petroff, CaMKII mediates angiotensin II-induced cardiomyocytes apoptosis: role of Ca2, ROS and p38 MAPK, J. Mol. Cell. Cardiol. 44 (2008) 764.
[20] C.J. Howe, M.M. Lahair, J.A. McCubrey, R.A. Franklin, Redox regulation of the calcium/calmodulin-dependent protein kinases, J. Biol. Chem. 279 (2004) 44573–44581.
[21] Z.A. Hing, R. Mantel, K.A. Beckwith, D. Guinn, E. Williams, L.L. Smith, K. Williams, A.J. Johnson, A.M. Lehman, J.C. Byrd, J.A. Woyach, R. Lapalombella, Selinexor is effective in acquired resistance to ibrutinib and synergizes with ibrutinib in chronic lymphocytic leukemia, Blood 125 (2015) 3128–3132.
[22] X.F. Hu, L. Wang, G. Xiang, W. Lei, Y.F. Feng, Angiogenesis impairment by the NADPH oxidase-triggered oxidative stress at the bone-implant interface: critical mechanisms and therapeutic targets for implant failure under hyperglycemic conditions in diabetes, Acta Biomater. 73 (2018) 470–487.
[23] N. Li, X.H. Wehrens, Programmed electrical stimulation in mice, J. Vis. Exp. 1730 (2010).
[24] J.M. Tuomi, P. Chidiac, D.L. Jones, Evidence for enhanced M3 muscarinic receptor function and sensitivity to atrial arrhythmia in the RGS2-deficient mouse, Am. J. Physiol. Heart Circ. Physiol. 298 (2010) H554–H561.
[25] J.M. Tuomi, K. Tyml, D.L. Jones, Atrial tachycardia/fibrillation in the connexin 43 G60S mutant (Oculodentodigital dysplasia) mouse, Am. J. Physiol. Heart Circ. Physiol. 300 (2011) H1402–H1411.
[26] J. Wang, N. Xu, X. Feng, N. Hou, J. Zhang, X. Cheng, Y. Chen, Y. Zhang, X. Yang, Targeted disruption of Smad4 in cardiomyocytes results in cardiac hypertrophy and heart failure, Circ. Res. 97 (2005) 821–828.
[27] F. Han, Y.M. Lu, H. Hasegawa, H. Kanai, E. Hachimura, Y. Shirasaki, K. Fukunaga, Inhibition of dystrophin breakdown and endothelial nitric-oxide synthase uncoupling accounts for cytoprotection by 3-[2-[4-(3-chloro-2-methylphenyl)-1-piperazinyl]ethyl]-5,6-dimethoxy-1-(4-imidazolylmethyl)-1H-indazole dihydrochloride 3.5 hydrate (DY-9760e) in left ventricular hypertrophied mice, J. Pharmacol. Exp. Ther. 332 (2010) 421–428 2010.
[28] N. Rizzi, N. Liu, C. Napolitano, A. Nori, F. Turcato, B. Colombi, S. Bicciato, D. Arcelli, A. Spedito, M. Scelsi, L. Villani, G. Esposito, S. Boncompagni, F. Protasi, P. Volpe, S.G. Priori, Unexpected structural and functional consequences of the R33Q homozygous mutation in cardiac calsequestrin: a complex arrhythmogenic cascade in a knock in mouse model, Circ. Res. 103 (2008) 298–306.
[29] M. Denegri, J.E. Avelino-Cruz, S. Boncompagni, S.A. De Simone, A. Auricchio, L. Villani, P. Volpe, F. Protasi, C. Napolitano, S.G. Priori, Viral gene transfer rescues arrhythmogenic phenotype and ultrastructural abnormalities in adult calsequestrin-null mice with inherited arrhythmias, Circ. Res. 110 (2012) 663–668.
[30] E. Mandache, L.M. Popescu, M. Gherghiceanu, Myocardial interstitial Cajal-like cells (ICLC) and their nanostructural relationships with intercalated discs: shed vesicles as intermediates, J. Cell Mol. Med. 11 (2007) 1175–1184.
[31] G.R. Sambrano, I. Fraser, H. Han, Y. Ni, T. O'Connell, Z. Yan, J.T. Stull, Navigating the signalling network in mouse cardiac myocytes, Nature 420 (2002) 712–714.
[32] J. Yu, L. Chen, B. Cui, C. Wu, M.Y. Choi, Y. Chen, L. Zhang, L.Z. Rassenti, G.F. Widhopf II, T.J. Kipps, Cirmtuzumab inhibits Wnt5a-induced Rac1 activation in chronic lymphocytic leukemia treated with ibrutinib, Leukemia 31 (2017) 1333–1339.
[33] J. Liu, Y. Zhu, S. Chen, B. Shen, F. Yu, Y. Zhang, R. Shen, Apocynin attenuates cobalt chloride induced pheochromocytoma cell apoptosis by inhibiting P38-MAPK/caspase-3 pathway, Cell. Physiol. Biochem. 48 (2018) 208–214.
[34] S. Roberge, J. Roussel, D.C. Andersson, A.C. Meli, B. Vidal, F. Blandel, J.T. Lanner, J.Y. Le Guennec, A. Katz, H. Westerblad, A. Lacampagne, J. Fauconnier, TNF-alpha-mediated caspase-8 activation induces ROS production and TRPM2 activation in

adult ventricular myocytes, Cardiovasc. Res. 103 (2014) 90–99.
[35] S. Zuo, L.L. Li, Y.F. Ruan, L. Jiang, X. Li, S.N. Li, S.N. Wen, R. Bai, N. Liu, X. Du, J.Z. Dong, C.S. Ma, Acute administration of tumour necrosis factor-a induces spontaneous calcium release via the reactive oxygen species pathway in atrial myocytes, Europace 20 (2018) 1367–1374.
[36] P.K. Smith, R.I. Krohn, G.T. Hermanson, A.K. Mallia, F.H. Gartner, M.D. Provenzano, E.K. Fujimoto, N.M. Goeke, B.J. Olson, D.C. Klenk, Measurement of protein using bicinchoninic acid, Anal. Biochem. 150 (1985) 76–85.
[37] G. Candiano, M. Bruschi, L. Musante, L. Santucci, G.M. Ghiggeri, B. Carnemolla, P. Orecchia, L. Zardi, P.G. Righetti, Blue silver: a very sensitive colloidal Coomassie G-250 staining for proteome analysis, Electrophoresis 25 (2004) 1327–1333.
[38] J.R. Wiśniewski, A. Zougman, N. Nagaraj, M. Mann, Filter-aided sample preparation (FASP) for MS-based proteomic analysis, Nat. Methods 6 (2009) 359–362 2009.
[39] M. Ashburner, C.A. Ball, J.A. Blake, D. Botstein, H. Butler, J.M. Cherry, A.P. Davis, K. Dolinski, S.S. Dwight, J.T. Eppig, M.A. Harris, D.P. Hill, L. Issel-Tarver, A. Kasarskis, S. Lewis, J.C. Matese, J.E. Richardson, M. Ringwald, G.M. Rubin, G. Sherlock, Gene ontology: tool for the unification of biology. The gene ontology consortium, Nat. Genet. 25 (2000) 25–29.
[40] D.W. Huang, B.T. Sherman, R.A. Lempicki, Systematic and integrative analysis of large gene lists using david bioinformatics resources, Nat. Protoc. 4 (2009) 44–57.
[41] F. Zhang, X. Xu, B. Zhou, Z. He, Q. Zhai, Gene expression profile change and associated physiological and pathological effects in mouse liver induced by fasting and refeeding, PLoS One 6 (2011) e27553.
[42] J.Y. Youn, J. Zhang, Y. Zhang, H. Chen, D. Liu, P. Ping, J.N. Weiss, H. Cai, Oxidative stress in atrial fibrillation: an emerging role of NADPH oxidase, J. Mol. Cell. Cardiol. 62 (2013) 72–79.
[43] E.D. Deeks, Ibrutinib: a review in chronic lymphocytic Leukaemia, Drugs 77 (2017) 225–236.
[44] G. Reda, B. Fattizzo, R. Cassin, V. Mattiello, T. Tonella, D. Giannarelli, F. Massari, A. Cortelezzi, Predictors of atrial fibrillation in ibrutinib treated CLL patients: a prospective study, J. Hematol. Oncol. 11 (2018) 79.
[45] C.P.S. Tang, J. McMullen, C. Tam, Cardiac side effects of bruton tyrosine kinase (BTK) inhibitors, Leuk. Lymphoma 59 (2018) 1554–1564.
[46] N. Li, T. Wang, W. Wang, M.J. Culter, Q. Wang, N. Voigt, D.S. Rosenbaum, D. Dobrev, X.H.T. Wehrens, Inhibition of CaMKII phosphorylation of RyR2 prevents induction of atrial fibrillation in FKBP12.6 knockout mice, Circ. Res. 110 (2012) 465–470.
[47] G.F. Tomaselli, A.S. Barth, Sudden cardio arrest: oxidative stress irritates the heart, Nat. Med. 16 (2010) 648–649.
[48] A. Purohit, A.G. Rokita, X. Guan, B. Chen, O.M. Koval, N. Voigt, S. Neef, T. Sowa, Z. Gao, E.D. Luczak, H. Stefansdottir, A.C. Behunin, N. Li, R.N. El-Accaoui, B. Yang, P.D. Swaminathan, R.M. Weiss, X.H. Wehrens, L.S. Song, D. Dobrev, L.S. Maier, M.E. Anderson, Oxidized Ca2+/calmodul independent protein kinase II triggers atrial fibrillation, Circulation 128 (2013) 1748–1757.
[49] J.A. Vest, X.H.T. Wehrens, S.R. Reiken, S.E. Lehnart, D. Dobrev, P. Chandra, P. Danilo, U. Ravens, M.R. Rosen, A.R. Marks, Defective cardiac ryanodine receptor fibrillation, Circulation 111 (2005) 2025–2032.
[50] I. Lenaerts, V. Bito, F.R. Heinzel, R.B. Driesen, P. Holemans, J. D'hooge, H. Heidbüchel, K.R. Sipido, R. Willems, Ultrastructural and functional remodeling of the coupling between Ca^{2+} influx and sarcoplasmic reticulum Ca^{2+} release in right atrial myocytes from experimental persistent atrial fibrillation, Circ. Res. 105 (2009) 876–885.
[51] A. El-Armouche, P. Boknik, T. Eschenhagen, L. Carrier, M. Knaut, U. Ravens, D. Dobrev, Molecular determinants of altered Ca^{2+} handling in human chronic atrial fibrillation, Circulation 114 (2006) 670–680.
[52] D. Dobrev, S. Nattel, Calcium handling abnormalities in atrial fibrillation as a target for innovative therapeutics, J. Cardiovasc. Pharmacol. 52 (2008) 293–299.
[53] S. Nattel, B. Burstein, D. Dobrev, Atrial remodeling and atrial fibrillation:mechanisms and implications, Circ. Arrhythmia Electrophysiol. (2008) 62–73.
[54] Y.H. Kao, Y.C. Chen, C.C. Cheng, T.I. Lee, Y.J. Chen, S.A. Chen, Tumor necrosis factor-α decreases sarcoplasmic reticulum Ca^{2+}-ATPase expressions via the promoter methylation in cardiomyocytes, Crit. Care Med. 38 (2010) 217–222.
[55] H. Musa, K. Kaur, R. O'Connell, M. Klos, G. Guerrero-Serna, U.M.R. Avula, T.J. Herron, J. Kalifa, J. Mb Anumonwo, J. Jalife, Inhibition of platelet-derived growth factor-AB signaling prevents electromechanical remodeling of adult atrial myocytes that contact myofibroblasts, Heart Rhythm 10 (2013) 1044–1051.
[56] G.A. Begg, A.V. Holden, G.Y. Lip, S. Plein, M.H. Tayebjee, Assessment of atrial fibrosis for the rhythm control of atrial fibrillation, Int. J. Cardiol. 220 (2016) 155–161.
[57] G. Gaudesius, M. Miragoli, S.P. Thomas, S. Rohr, Coupling of cardiac electrical activity over extended distances by fibroblasts of cardiac origin, Circ. Res. 93 (2003) 421–428.
[58] S. Jong, T. Veen, H. Rijen, J. Bakker, Fibrosis and cardiac arrhythmias, J. Cardiovasc. Pharmacol. 57 (2011) 630–638.
[59] M.J. Mihm, F. Yu, C.A. Carnes, P.J. Reiser, P.M. McCarthy, D.R. Van Wagoner, J.A. Bauer, Impaired myofibrillar energetics and oxidative injury during human atrial fibrillation, Circulation 104 (2001) 174–180.
[60] R. Khan, R. Sheppard, Fibrosis in heart disease: understanding the role of transforming growth factor-beta in cardiomyopathy, valvular disease and arrhythmia, Immunology 118 (2006) 10–24.
[61] S. Verheule, T. Sato, T. Everett, S.K. Engle, D. Otten, M. Rubart-von der Lohe, H.O. Nakajima, H. Nakajima, L.J. Field, J.E. Olgin, Increased vulnerability to atrial fibrillation in transgenic mice with selective atrial fibrosis caused by overexpression of TGF-beta1, Circ. Res. 94 (2004) 1458–1465.
[62] G. Lamirault, N. Gaborit, N.L. Meur, C. Chevalier, G. Lande, S. Demolombe, D. Escande, S. Nattel, J.J. Léger, M. Steenman, Gene expression profile associated with chronic atrial fibrillation and underlying valvular heart disease in man, J. Mol. Cell. Cardiol. 40 (2006) 173–184.
[63] Y.H. Yeh, C.T. Kuo, G.J. Chang, X.Y. Qi, S. Nattel, W.J. Chen, Nicotinamide adenine dinucleotide phosphate oxidase 4 mediates the differential responsiveness of atrial versus ventricular fibroblasts to transforming growth factor-beta, Circ. Arrhythmia Electrophysiol. 6 (2013) 790–798.
[64] H. Cai, K.K. Griendling, D.G. Harrison, The vascular NAD(P)H oxidases as therapeutic targets in cardiovascular diseases, Trends Pharmacol. Sci. 24 (2003) 471–478.
[65] A. Kunamalla, J. Ng, V. Parini, S. Yoo, K.A. McGee, T.T. Tomson, D. Gordon, E.B. Thorp, J. Lomasney, Q. Zhang, S. Shah, S. Browne, B.P. Knight, R. Passman, J.J. Goldberger, G. Aistrup, R. Arora, Constitutive expression of a dominant negative TGF-β type II receptor in the posterior left atrium leads to beneficial remodeling of atrial fibrillation substrate, Circ. Res. 119 (2016) 69–82.
[66] L. Harling, S. Rasoli, J.A. Vecht, H. Ashrafian, A. Kourliouros, T. Athanasiou, Do antioxidant vitamins have an anti-arrhythmic effect following cardiac surgery? A meta-analysis of randomised controlled trials, Heart 97 (2011) 1636–1642.
[67] M.F. McCarty, Practical prevention of cardiac remodeling and atrial fibrillation with full-spectrum antioxidant therapy and ancillary strategies, Med. Hypotheses 75 (2010) 141–147.
[68] R. Bhuriya, M. Singh, A. Sethi, J. Molnar, A. Bahekar, P.P. Singh, S. Khosla, R. Arora, Prevention of recurrent atrial fibrillation with angiotensin-converting enzyme inhibitors or angiotensin receptor blockers: a systematic review and meta-analysis of randomized trials, J. Cardiovasc. Pharmacol. Ther. 16 (2011) 178–184.
[69] G. Huang, J.B. Xu, J.X. Liu, Y. He, X.L. Nie, Q. Li, Y.M. Hu, S.Q. Zhao, M. Wang, W.Y. Zhang, X.R. Liu, T. Wu, A. Arkin, T.J. Zhang, Angiotensin-converting enzyme inhibitors and angiotensin receptor blockers decrease the incidence of atrial fibrillation: a meta-analysis, Eur. J. Clin. Investig. 41 (2011) 719–733.
[70] J. Stolk, T.J. Hiltermann, J.H. Dijkman, A.J. Verhoeven, Characteristics of the inhibition of NADPH oxidase activation in neutrophils by apocynin, a methoxy-substituted catechol, Am. J. Respir. Cell Mol. Biol. 11 (1994) 95–102.
[71] F. Qin, M. Simeone, R. Patel, Inhibition of NADPH oxidase reduces myocardial oxidative stress and apoptosis and improves cardiac function in heart failure after myocardial infarction, Free Radic. Biol. Med. 43 (2007) 271–281.
[72] A.A. Sovari, N. Morita, H.S. Karagueuzian, Apocynin: a potent NADPH oxidase inhibitor for the management of atrial fibrillation, Redox Rep. 13 (2008) 242–245.
[73] C.T. Tsai, C.D. Tseng, J.J. Hwang, C.K. Wu, C.C. Yu, Y.C. Wang, W.P. Chen, L.P. Lai, F.T. Chiang, J.L. Lin, Tachycardia of atrial myocytes induces collagen expression in atrial fibroblasts through transforming growth factor beta1, Cardiovasc. Res. 89 (2011) 805–815.
[74] M.M. Elahi, S. Flatman, B.M. Matata, Tracing the origins of postoperative atrial fibrillation: the concept of oxidative stress-mediated myocardial injury phenomenon, Eur. J. Cardiovasc. Prev. Rehabil. 15 (2008) 735–741.
[75] E.G. Daoud, B.P. Knight, R. Weiss, M. Bahu, W. Paladino, R. Goyal, K.C. Man, S.A. Strickberger, F. Morady, Effect of verapamil and procainamide on atrial fibrillation-induced electrical remodeling in humans, Circulation 96 (1997) 1542–1550.
[76] Y.M. Kim, T.J. Guzik, Y.H. Zhang, M.H. Zhang, H. Kattach, C. Ratnatunga, R. Pillai, K.M. Channon, B. Casadei, A myocardial Nox2 containing NAD(P)H oxidase contributes to oxidative stress in human atrial fibrillation, Circ. Res. 97 (2005) 629–636.
[77] D.X. Zhang, K. Ren, Y. Guan, Y.T. Wang, Z.L. Shan, Protective effects of apocynin on atrial electrical remodeling and oxidative stress in a rabbit rapid atrial pacing model, Chin. J. Physiol. 57 (2014) 76–82.
[78] J.R. Erickson, B.J. He, I.M. Grumbach, M.E. Anderson, CaMKII in the cardiovascular system: sensing redox states, Physiol. Rev. 91 (2011) 889–915.
[79] L.H. Xie, F. Chen, H.S. Karagueuzian, J.N. Weiss, Oxidative-stress-induced afterdepolarizations and calmodulin kinase II signaling, Circ. Res. 104 (2009) 79–86.
[80] M.G. Chelu, S. Sarma, S. Sood, S. Wang, R.J. van Oort, D.G. Skapura, N. Li, M. Santonastasi, F.U. Müller, W. Schmitz, U. Schotten, M.E. Anderson, M. Valderrábano, D. Dobrev, X.H.T. Wehrens, Calmodulin kinase IImediated sarcoplasmic reticulum Ca^{2+} leak promotes atrial fibrillation in mice, J. Clin. Investig. 119 (2009) 1940–1951.
[81] N. Li, T. Wang, W. Wang, M.J. Cutler, Q. Wang, N. Voigt, D.S. Rosenbaum, D. Dobrev, X.H. Wehrens, Inhibition of CaMKII phosphorylation of RyR2 prevents induction of atrial fibrillation in FKBP12.6 knockout mice, Circ. Res. 110 (2012) 465–470.
[82] E.D. Luczak, M.E. Anderson, CaMKII oxidative activation and the pathogenesis of cardiac disease, J. Mol. Cell. Cardiol. 73 (2014) 112–116.
[83] N. Li, D.Y. Chiang, S. Wang, Q. Wang, L. Sun, N. Voigt, J.L. Respress, S. Ather, D.G. Skapura, V.K. Jordan, F.T. Horrigan, W. Schmitz, F.U. Müller, M. Valderrabano, S. Nattel, D. Dobrev, X.H.T. Wehrens, Ryanodine receptor–mediated calcium leak drives progressive development of an atrial fibrillation substrate in a transgenic mouse model, Circulation 129 (2014) 1276–1285.
[84] J. Shan, W. Xie, M. Betzenhauser, S. Reiken, B. Chen, A. Wronska, A.R. Marks, Calcium leak through ryanodine receptors leads to atrial fibrillation in 3 mouse models of catecholaminergic polymorphic ventricular tachycardia, Circ. Res. 111 (2012) 708–717.
[85] N. Voigt, N. Li, Q. Wang, W. Wang, A.W. Trafford, I. Abu-Taha, Q. Sun, T. Wieland, U. Ravens, S. Nattel, X.H.T. Wehrens, D. Dobrev, Enhanced sarcoplasmic reticulum Ca^{2+} leak and increased Na^{+}-Ca^{2+} exchanger function underlie delayed afterdepolarizations in patients with chronic atrial fibrillation, Circulation 125 (2012) 2059–2070.